

Libcint: An efficient general integral library for Gaussian basis functions

Qiming Sun*

Department of Chemistry, Princeton University, Princeton NJ 08544

E-mail: osirpt.sun@gmail.com

Abstract

An efficient integral library Libcint was designed to automatically implement general integrals for Gaussian-type scalar and spinor basis functions. The library can handle arbitrary integral expressions on top of \mathbf{p} , \mathbf{r} and σ operators with one-electron overlap and nuclear attraction, two-electron Coulomb and Gaunt operators. Using a symbolic algebra tool, new integrals are derived and translated to C code programmatically. The generated integrals can be used in various types of molecular properties. In the present work, we computed the analytical gradients and NMR shielding constants at both non-relativistic and four-component relativistic Hartree-Fock level to demonstrate the capability of the integral library. Due to the use of kinetically balanced basis and gauge including atomic orbitals, the relativistic analytical gradients and shielding constants requires the integral library to handle the fifth-order electron repulsion integral derivatives. The generality of the integral library is achieved without losing efficiency. On the modern multi-CPU platform, Libcint can easily reach the overall throughput being many times of the I/O bandwidth. On a 20-core node, we are able to achieve an average output 7.9 GB/s for C_{60} molecule with cc-pVTZ basis.

*To whom correspondence should be addressed

1 Introduction

In computational chemistry, evaluation of integrals is the ground of modeling the molecular electronic structure and various types of molecular properties. Because of the importance of integrals, a considerable number of researches have been devoted on the efficient algorithm to evaluate the two-electron repulsion integrals (ERI) over Gaussian functions¹⁻¹⁸ since Boys' work¹ in 1950. Grounded on the Rys-quadrature method which was developed by Dupuis, Rys, and King (DRK),^{2,3} Pople and Hehre⁴ developed an efficient method for highly contracted *s* and *p* functions. To reduce the number of floating-point operations (FLOPS) required by the quadrature integration technique, Obara and Saika proposed a recurrence relation⁶⁻⁸ (RR) for the 6D-integral rather than the 2D-integral of the original DRK's algorithm. Based on OS's formula, an early contraction scheme was proposed by Gill, Head-Gordon and Pople¹⁰⁻¹³ (HGP). Their formula transferred the RR out of the contraction loops and further reduced FLOPS. Although OS's method as well as HGP's early contraction scheme required less FLOPS counts, they are less efficient than DRK's 2D-integral algorithm in some scenario for low degree of contraction due to the complex formula in their algorithm.¹⁴ Lindh, Ryu, and Liu^{14,15} first noticed this problem and proposed a compromised scheme. Dupuis and Marquez¹⁶ combined the advantages of DRK, HGP etc. algorithms to optimize the FLOPS counts. Besides these applications, Ishida's ACE algorithm^{17,18} also achieved attractive FLOPS counts.

Most of the existed integral algorithms focused on the FLOPS counts which only provide the theoretical computing efficiency. It remains a challenge to implement new types of integrals cost-effectively in both the human labour and the real computational efforts. One source of the new integrals is the calculation of molecular properties such as¹⁹ response theory, which requires the differentiated integrals.²⁰ Perturbation-dependent basis technique,²¹⁻²³ e.g. gauge including atomic orbitals^{21,22} (GIAO) also introduces the complications on the evaluation of integrals. Inclusion of relativistic effect is another source that brings new integrals.^{19,24-27} It is very common in relativistic quantum chemistry to evaluate high-order integrals, e.g. Breit-Pauli Hamiltonian^{28,29} introduces many one-electron and two-electron operators in terms of the product of \mathbf{p} and \mathbf{r} op-

erators. One basic assumption in four-component relativistic theory is the balanced treatment of large and small components.^{25,30–32} It results in various types of kinetic (magnetic) balance conditions^{25–27,33–35} and the corresponding one-electron and two-electron j -adapted (spinor) integrals. It is a heavy task to manually implement new code to efficiently evaluate every new type of integrals.

To implement an efficient integral program, the architecture of modern computer is another important subject that should be taken into account.^{36,37} The efficiency of an algorithm is not merely determined by the necessary FLOPS. A well optimized code can take full advantage of computer architecture, such as the single instruction multiple data (SIMD) units, to achieve instruction level parallelization.³⁸ Data locality can also affect program efficiency since the modern computer hardware favours simple data structure which are local and aligned in the memory. As such, it is non-trivial to translate an integral algorithm to a real-world efficient implementation.^{36,37,39–41}

Targeting to efficiently provide new integrals, an open-source and general purposed integral library Libcint⁴² was designed. In this library, a built-in symbolic algebra system can parse the integral expression which is the polynomial of \mathbf{p} operator, \mathbf{r} operator and Pauli matrices σ and decompose the expressions to the basic Cartesian integrals. The basic Cartesian ERI are evaluated with DRK's algorithm. There are two reasons we made this choice. (i) the intermediates for the derived integrals and the basic ERIs have the similar structure in the DRK's 2D-integral framework. It allows us to reuse most of the code which has been highly optimized for the basic ERIs. It also reduces the complexity of the code generator. (ii) we observed that the data structure of DRK's algorithm shows high locality which is easy to be fit into the CPU Cache structure. To cope with j -adapted spinor integrals for the four-component and two-component relativistic theory, the symbolic program can pick a proper function to assemble the intermediate Cartesian integrals.

In this paper, we describe the detail of the integral generation algorithm in Section 2. As a numerical example, we computed analytical nuclear gradients and NMR shielding constants for $\text{Cr}(\text{CO})_6$ and UF_6 molecule. They are presented in Section 3. The performances of spherical and spinor integrals for ethane molecule with double, triple and quadruple zeta bases are tested and

compared in Section 4.

2 Algorithm

The evaluation of integral can be divided into two separate steps. First is to calculate all kinds of primitive intermediate Cartesian integrals. Second step is to assemble and contract the intermediates, then transform them to the real spherical or spinor representations. In the following paragraphs, we will use the superscripts C , S and J to denote the integrals in the Cartesian, spherical and j -adapted spinor representations.

In the first step, we implemented a symbolic algebra program to parse the integral expression and formulate the intermediates. As shown in Table 1, the supported operators are classified into three classes: scalar, vector, and compound. The scalar and vector operators are the basic operators. The compound operators can be expressed in terms of the basic operators. In order to handle the Pauli matrices, we used quaternion

$$\sigma_x = \begin{pmatrix} 0 & 1 \\ 1 & 0 \end{pmatrix}, \quad \sigma_y = \begin{pmatrix} 0 & -i \\ i & 0 \end{pmatrix}, \quad \sigma_z = \begin{pmatrix} 1 & 0 \\ 0 & -1 \end{pmatrix}, \quad \mathbf{1}_{2 \times 2} = \begin{pmatrix} 1 & 0 \\ 0 & 1 \end{pmatrix}$$

as the fundamental structure to represent the scalar and vector operators. A scalar operator can be written as

$$q = q^x \sigma_x + q^y \sigma_y + q^z \sigma_z + q^1 \mathbf{1}_{2 \times 2}$$

A vector operator contains three quaternions

$$\vec{q} = q_x \mathbf{e}_x + q_y \mathbf{e}_y + q_z \mathbf{e}_z$$

Although many zeros might be introduced due to the quaternion representation, the evaluation of the quaternion expression is simple. An valid quaternion expression can only have three kinds of

basic contractions: dot product,

$$\vec{q}_a \cdot \vec{q}_b = q_{a,x}q_{b,x} + q_{a,y}q_{b,y} + q_{a,z}q_{b,z} \quad (1)$$

cross product,

$$\vec{q}_a \times \vec{q}_b = (q_{a,y}q_{b,z} - q_{a,z}q_{b,y})\mathbf{e}_x + (q_{a,z}q_{b,x} - q_{a,x}q_{b,z})\mathbf{e}_y + (q_{a,x}q_{b,y} - q_{a,y}q_{b,x})\mathbf{e}_z \quad (2)$$

and direct product

$$q_a \vec{q}_b = q_a q_{b,x} \mathbf{e}_x + q_a q_{b,y} \mathbf{e}_y + q_a q_{b,z} \mathbf{e}_z \quad (3)$$

$$\vec{q}_a q_b = q_{a,x} q_b \mathbf{e}_x + q_{a,y} q_b \mathbf{e}_y + q_{a,z} q_b \mathbf{e}_z \quad (4)$$

$$\begin{aligned} \vec{q}_a \vec{q}_b &= q_{a,x} q_{b,x} \mathbf{e}_x \mathbf{e}_x + q_{a,x} q_{b,y} \mathbf{e}_x \mathbf{e}_y + q_{a,x} q_{b,z} \mathbf{e}_x \mathbf{e}_z \\ &+ q_{a,y} q_{b,x} \mathbf{e}_y \mathbf{e}_x + q_{a,y} q_{b,y} \mathbf{e}_y \mathbf{e}_y + q_{a,y} q_{b,z} \mathbf{e}_y \mathbf{e}_z \\ &+ q_{a,z} q_{b,x} \mathbf{e}_z \mathbf{e}_x + q_{a,z} q_{b,y} \mathbf{e}_z \mathbf{e}_y + q_{a,z} q_{b,z} \mathbf{e}_z \mathbf{e}_z \end{aligned} \quad (5)$$

where the quaternion multiplication $q_a q_b$ can be expanded in terms of the Dirac relation

$$\boldsymbol{\sigma} \cdot \mathbf{A} \boldsymbol{\sigma} \cdot \mathbf{B} = \mathbf{A} \cdot \mathbf{B} + i \boldsymbol{\sigma} \cdot \mathbf{A} \times \mathbf{B}$$

$$q_a q_b = q_c = q_c^x \boldsymbol{\sigma}_x + q_c^y \boldsymbol{\sigma}_y + q_c^z \boldsymbol{\sigma}_z + q_c^1 \mathbf{1}_{2 \times 2} \quad (6)$$

$$q_c^x = i q_a^y q_b^z - i q_a^z q_b^y + q_a^x q_b^1 + q_a^1 q_b^x$$

$$q_c^y = i q_a^z q_b^x - i q_a^x q_b^z + q_a^y q_b^1 + q_a^1 q_b^y$$

$$q_c^z = i q_a^x q_b^y - i q_a^y q_b^x + q_a^z q_b^1 + q_a^1 q_b^z$$

$$q_c^1 = q_a^x q_b^x + q_a^y q_b^y + q_a^z q_b^z + q_a^1 q_b^1$$

However, a special treatment is needed for the Gaunt interactions

$$\frac{\alpha_1 \cdot \alpha_2}{r_{12}}, \quad \alpha = \begin{pmatrix} 0 & \sigma \\ \sigma & 0 \end{pmatrix}$$

The two α operators in the Gaunt operator belongs to the different electrons. We cannot use Eq. (6) to simplify the dot product. Instead, it was decomposed to three components. The three components are calculated separately and summed up at last.

By recursively calling the contractions and quaternion products (1) - (6), we are able to derive the expressions of all possible Cartesian intermediates for all tensor components. E.g. the symbolic program can generate in total six Cartesian intermediates for $(a \sigma \times \mathbf{p}b|cd)^J$ which comes with three Cartesian tensor components

$$\begin{aligned} (a \sigma \times \mathbf{p}b|cd)_x^J &: -i(a \nabla_z b|cd)^C \sigma_y, \quad i(a \nabla_y b|cd)^C \sigma_z, \\ (a \sigma \times \mathbf{p}b|cd)_y^J &: -i(a \nabla_x b|cd)^C \sigma_z, \quad i(a \nabla_z b|cd)^C \sigma_x, \\ (a \sigma \times \mathbf{p}b|cd)_z^J &: -i(a \nabla_y b|cd)^C \sigma_x, \quad i(a \nabla_x b|cd)^C \sigma_y. \end{aligned}$$

Next thing the symbolic program did is to translate the expression of Cartesian intermediates to C code. Following DRK's method, a Cartesian integral can be evaluated as the inner product of three two-dimensional integrals I_x, I_y, I_z with certain weights w_i

$$\text{ERI} = \int_0^\infty I_x I_y I_z du = \sum_i w_i I_x(i) I_y(i) I_z(i). \quad (7)$$

When an integral expression contains ∇ or \mathbf{r} operators, we need to employ

$$\begin{aligned} \frac{\partial}{\partial x} \phi_a^x &= n_a^x (x - X_A)^{n_a^x - 1} e^{-\alpha_a (x - X_A)^2} - 2\alpha_a (x - X_A)^{n_a^x + 1} e^{-\alpha_a (x - X_A)^2} \\ x \phi_a^x &= X_A (x - X_A)^{n_a^x} e^{-\alpha_a (x - X_A)^2} + (x - X_A)^{n_a^x + 1} e^{-\alpha_a (x - X_A)^2} \end{aligned}$$

to transfer the four-index 2D integral $I_x^{(ab|cd)}$ to another four-index 2D integral $\tilde{I}_x^{(ab|cd)}$ which is a

Table 1: The operators supported by Libcint library

Operators	Class	Expression
∇_x	Scalar	
∇_y	Scalar	
∇_z	Scalar	
p_x	Compound	$-i\nabla_x$
p_y	Compound	$-i\nabla_y$
p_z	Compound	$-i\nabla_z$
x	Scalar	
y	Scalar	
z	Scalar	
σ_x	Scalar	
σ_y	Scalar	
σ_z	Scalar	
$\frac{1}{ r-R }$	Scalar	
$\frac{1}{r_{12}}$	Scalar	
∇	Vector	
\mathbf{p}	Compound	$-i\nabla$
\mathbf{r}	Vector	
σ	Vector	
$\frac{\mathbf{r}-\mathbf{R}}{ \mathbf{r}-\mathbf{R} ^3}$	Compound	$-\nabla \frac{1}{ \mathbf{r}-\mathbf{R} }$
$\hat{g}_{\mu\nu}$	Compound	$i(\mathbf{R}_\mu - \mathbf{R}_\nu) \times \mathbf{r}$
Gaunt-like	Compound	$\frac{\sigma_1 \cdot \sigma_2}{r_{12}}$

linear combination of a lower and a higher 2D integrals,

$$\begin{aligned}
I_x^{(\nabla_x ab|cd)} &= n_a^x I_x^{(a-1 b|cd)} - 2\alpha_a I_x^{(a+1 b|cd)} \\
I_x^{(x ab|cd)} &= X_A I_x^{(ab|cd)} + I_x^{(a+1 b|cd)}
\end{aligned} \tag{8}$$

According to these relations, we are able to build the derived 2D integrals \tilde{I}_x in an ‘‘assembling’’ subroutine which consumes one ∇ or \mathbf{r} then form a derived 2D integral once at a time. If the integral contains two or more operators, the assembling subroutine needs to be invoked recursively until all operators are consumed.

It should be noted that the order we applied relations (8) is opposite to the natural order we manipulate the operators. To apply a list of operators to a function, the natural order starts from the rightmost operator. But in the assembling subroutine, relations (8) are invoked from the leftmost operator. E.g. in terms of the natural order, the leftmost derivative operator of $\nabla_x x \nabla_x \nabla_x \phi_a^x$ can produce a factor $4\alpha_a^2(n_a^x + 3)$

	∇_x	x	∇_x	∇_x	ϕ_a^x
momentum index	$n_a^x + 2$	$n_a^x + 3$	$n_a^x + 2$	$n_a^x + 1$	n_a^x
factor	$4\alpha_a^2(n_a^x + 3)$	$4\alpha_a^2$	$4\alpha_a^2$	$-2\alpha_a$	1

where the momentum index of the Gaussian function $\phi_a^x = (x - X_A)^{n_a^x} e^{-\alpha_a(x - X_A)^2}$ stands for the exponential of the polynomial part $(x - X_A)^{n_a^x}$. By calling relations (8), left-to-right propagation can produce the same factor

$$\begin{aligned}
&\nabla_x \ x \ \nabla_x \ \nabla_x \ I_x^{(ab|cd)} \\
I_x^{[1]}(n) &= \underline{n_a^x} I_x^{(a-1 b|cd)} - 2\alpha_a I_x^{(a+1 b|cd)} \\
I_x^{[2]}(n) &= I_x^{[1]}(n+1) + X_A I_x^{[1]}(n) = \underline{(n_a^x + 1)} I_x^{(ab|cd)} + \dots \\
I_x^{[3]}(n) &= -2\alpha_a I_x^{[2]}(n+1) + n I_x^{[2]}(n-1) = \underline{-2\alpha_a(n_a^x + 2)} I_x^{(a+1 b|cd)} + \dots \\
I_x^{[4]}(n) &= -2\alpha_a I_x^{[3]}(n+1) + n I_x^{[3]}(n-1) = \underline{4\alpha_a^2(n_a^x + 3)} I_x^{(a+2 b|cd)} + \dots
\end{aligned}$$

Applying similar analysis to all other terms, we found the same observation on the application orders: The correct factor can only be produced by the left-to-right order with the relations (8).

In the second step, the transformations of Cartesian to spherical or Cartesian to spinor were hard-coded in the program. There are eight kinds of transformations for the spinor integrals, which are arose from the combinations of three conditions:

- Which electron to transform. The four indices in $(ab|cd)^J$ are be grouped into two sets ab and cd .
- Whether the integral expression has Pauli matrices. E.g. $(\sigma\mathbf{p}a\ \sigma\mathbf{p}b|cd)^J$ contains Pauli matrices, but $(a\ \sigma\mathbf{p}\sigma\mathbf{p}b|cd)^J$ does not because $\sigma\mathbf{p}\sigma\mathbf{p} = p^2$.
- Which phase the integral is associated with, 1 or i . E.g. $(a\ \sigma \times \mathbf{p}b|cd)^J$ has a phase factor i from operator \mathbf{p} .

For a given integral expression, the symbolic program needs to identify the transformation from the above three conditions and choose the proper transformation subroutines to execute.

3 Computational examples

In this section, we present the numerical examples for the integrals implemented with Libcint library. We used Pyscf⁴² program package to call the integral library and calculate the ground state energy, analytical nuclear gradients and NMR shielding constants for $\text{Cr}(\text{CO})_6$ and UF_6 molecule at non-relativistic and 4-component (4C) relativistic (Dirac-Coulomb Hamiltonian) mean field level. We used cc-pVTZ basis for Cr, C, O and F, Dyall triple-zeta set⁴³ for U. In the 4C relativistic calculations, we uncontracted the basis of Cr atom to get better description of the core electrons. For the relativistic ground state and nuclear gradients, we employed the restrict kinetically balanced (RKB) basis sets, which introduces the $\sigma \cdot \mathbf{p}|a\rangle$ basis functions. For NMR properties, we employed

magnetic-field-dependent basis functions. They are GIAOs for non-relativistic Hamiltonian

$$-\frac{i}{2}\mathbf{B} \times \mathbf{R}_a \cdot \mathbf{r}|a\rangle$$

and magnetically balanced RMB-GIAOs basis for relativistic Hamiltonian

$$\begin{aligned} &-\frac{i}{2}\mathbf{B} \times \mathbf{R}_a \cdot \mathbf{r}|a\rangle \quad \text{for large components} \\ &\left(\frac{1}{2}\mathbf{B} \times \mathbf{r} \cdot \boldsymbol{\sigma} - \frac{i}{2}\mathbf{B} \times \mathbf{R}_a \cdot \mathbf{r}\right)|a\rangle \quad \text{for small components} \end{aligned}$$

The magnetically balanced basis naturally introduces the dia-magnetic contributions to the relativistic NMR theory, which is comparable to the dia-magnetic terms in the non-relativistic calculations. Since the theory of the relativistic analytic gradients and magnetic properties is out of the scope of present paper, we refer the readers to the literatures^{26,32,44–47} for more theoretical details.

Table 2 documents all the 49 types of integrals which are required in these calculations. Due to the use of RKB and RMB-GIAO basis, relativistic theory brings more integrals than that appeared in the non-relativistic theory. The non-relativistic computation only needs 3 types of two-electron spherical integrals while the relativistic framework needs 13 types of two-electron spinor integrals. Among the 13 types, $(\nabla\sigma\mathbf{p}a \sigma\mathbf{p}b|\sigma\mathbf{p}c \sigma\mathbf{p}d)$ and $(\hat{g}_{ab}\sigma\mathbf{p}a \sigma\mathbf{p}b|\sigma\mathbf{p}c \sigma\mathbf{p}d)$ virtually require the fifth order derivative, which causes the relativistic computation being about 100 times slower than the corresponding non-relativistic computation (see more discussions in Section 4).

Table 3 and 4 are the results of the ground HF energies analytical nuclear gradients and the isotopic NMR shielding constants for both the non-relativistic and the 4C Dirac-Coulomb relativistic Hamiltonian.

By fixing the C-O bond at 1.140 Å,⁴⁸ we optimized the geometry, particularly, the Cr-C bond length in terms of the HF nuclear gradients. The equilibrium Cr-C bond length based on the non-relativistic Hamiltonian is 2.0106 Å. The relativistic effects strengthen the Cr-C bond and shorten it to 1.998 Å. On the contrary, the relativistic effects increase the U-F bond length from 1.977 Å to 1.983 Å.

Table 2: Integral types for ground state, analytical nuclear gradients and NMR shielding constants.

Hamiltonian	Non-relativistic	4C Dirac-Coulomb
ground HF	$\langle a b\rangle^S$	$\langle a b\rangle^J$
	$\langle a \nabla^2 b\rangle^S$	$\langle a \nabla^2 b\rangle^J$
	$\langle a \frac{Z_N}{r_N} b\rangle^S$	$\langle a \frac{Z_N}{r_N} b\rangle^J$
		$\langle \sigma\mathbf{p}a \frac{Z_N}{r_N} \sigma\mathbf{p}b\rangle^J$
	$(ab cd)^S$	$(ab cd)^J$ $(\sigma\mathbf{p}a\ \sigma\mathbf{p}b cd)^J$ $(\sigma\mathbf{p}a\ \sigma\mathbf{p}b \sigma\mathbf{p}c\ \sigma\mathbf{p}d)^J$
gradients	$\langle \nabla a b\rangle^S$	$\langle \nabla a b\rangle^J$
	$\langle \nabla a \nabla^2 b\rangle^S$	$\langle \nabla a \nabla^2 b\rangle^J$
	$\langle \nabla a \frac{Z_N}{r_N} b\rangle^S$	$\langle \nabla a \frac{Z_N}{r_N} b\rangle^J$
		$\langle \nabla\sigma\mathbf{p}a \frac{Z_N}{r_N} \sigma\mathbf{p}b\rangle^J$
	$\langle a (\nabla\frac{Z_N}{r_N}) b\rangle^S$	$\langle a (\nabla\frac{Z_N}{r_N}) b\rangle^J$
		$\langle \sigma\mathbf{p}a \nabla(\frac{Z_N}{r_N}) \sigma\mathbf{p}b\rangle^J$
	$(\nabla a\ b cd)^S$	$(\nabla a\ b cd)^J$ $(\nabla\sigma\mathbf{p}a\ \sigma\mathbf{p}b cd)^J$ $(\sigma\mathbf{p}a\ \sigma\mathbf{p}b \nabla c\ d)^J$ $(\nabla\sigma\mathbf{p}a\ \sigma\mathbf{p}b \sigma\mathbf{p}c\ \sigma\mathbf{p}d)^J$
NMR shielding	$\langle a \frac{\mathbf{r}\mathbf{r}}{r^3} b\rangle^S$	$\langle \mathbf{r}\times\sigma a \frac{\mathbf{r}\times\sigma}{r^3} b\rangle^J$
	$\langle a \frac{\mathbf{r}\times\mathbf{p}}{r^3} b\rangle^S$	$\langle a \frac{\mathbf{r}\times\sigma}{r^3} \sigma\mathbf{p}b\rangle^J$
	$\langle a \mathbf{r}\times\mathbf{p} b\rangle^S$	$\langle \mathbf{r}\times\sigma a \sigma\mathbf{p}b\rangle^J$
		$\langle \mathbf{r}\times\sigma a \frac{Z_N}{r_N} \sigma\mathbf{p}b\rangle^J$
	$\langle \hat{g}_{aba} b\rangle^S$	$\langle \hat{g}_{aba} b\rangle^J$
	$\langle \hat{g}_{aba} \nabla^2 b\rangle^S$	$\langle \hat{g}_{ab}\sigma\mathbf{p}a \sigma\mathbf{p}b\rangle^J$
	$\langle \hat{g}_{aba} \frac{Z_N}{r_N} b\rangle^S$	$\langle \hat{g}_{aba} \frac{Z_N}{r_N} b\rangle^J$
		$\langle \hat{g}_{ab}\sigma\mathbf{p}a \frac{Z_N}{r_N} \sigma\mathbf{p}b\rangle^J$
	$\langle \hat{g}_{aba} \frac{\mathbf{r}\times\mathbf{p}}{r^3} b\rangle^S$	$\langle \hat{g}_{ab}\sigma\mathbf{p}a \frac{\mathbf{r}\times\sigma}{r^3} b\rangle^J$
	$(\hat{g}_{aba}\ b cd)^S$	$(\hat{g}_{aba}\ b cd)^J$ $(\hat{g}_{ab}\sigma\mathbf{p}a\ \sigma\mathbf{p}b cd)^J$ $(\sigma\mathbf{p}a\ \sigma\mathbf{p}b \hat{g}_{cd}c\ d)^J$ $(\hat{g}_{ab}\sigma\mathbf{p}a\ \sigma\mathbf{p}b \sigma\mathbf{p}c\ \sigma\mathbf{p}d)^J$ $(\mathbf{r}\times\sigma a\ \sigma\mathbf{p}b cd)^J$ $(\mathbf{r}\times\sigma a\ \sigma\mathbf{p}b \sigma\mathbf{p}c\ \sigma\mathbf{p}d)^J$

The non-relativistic total shielding for chromium is -5718.5 ppm, which is far below the DFT value 507 ppm.⁴⁹ In contrast to the observation of the ZORA (zeroth order regular approximation) DFT simulation⁴⁹ which found that the relativistic effects decrease the shielding constants, our 4C RMB-GIAO computation increases the shielding to -4622.5 ppm. Note that the HF exchange is a big source of the paramagnetism. When we switch off the HF exchange in the coupled perturbation Hartree-Fock solver, the total shielding becomes 999.7 ppm in the 4C relativistic theory and 937.2 ppm in the non-relativistic theory. As expected, the shielding constants provided by DFT simulation lie between the full-exchange and the none-exchange limits. For uranium in UF_6 molecule, we can observe the similar trend that the relativistic effects increase the para-magnetism. An interesting phenomenon is the huge increment due to the relativistic effects which even changes the sign of the total magnetic shielding parameter, from the deshielding effect in the non-relativistic theory to a shielding effect.

Table 3: Hartree-Fock ground state energy, nuclear gradients (for Cr-C bond length, C-O bond was fixed at 1.140\AA), and NMR shielding constants of $Cr(CO)_6$.

	Non-relativistic	Dirac-Coulomb	ref
Energy gradients with respect to Cr-C bond length			
1.996 \AA		0.000464	
1.998 \AA		-0.000087	
2.000 \AA		-0.000286	
2.008 \AA	0.000453		
2.010 \AA	0.000096		
2.012 \AA	-0.000258		
$r_e / \text{\AA}$	2.0106	1.998	1.918 ^a , 1.998 ^b
HF energy / au	-1719.9158	-1729.8110	
NMR shielding / ppm			
Cr σ^{dia}	1815.0	1819.2	1801 ^c
Cr σ^{para}	-7533.5	-6441.7	-2419^c
Cr σ^{tot}	-5718.5	-4622.5	

^a Experimental data from reference 50.

^b Reference 51.

^c Reference 52. All electron ZORA with TZ/QZ basis.

Table 4: Hartree-Fock ground state energy, nuclear gradients (for U-F bond length) and NMR shielding constants of UF₆.

	Non-relativistic	Dirac-Coulomb	ref
Energy gradients with respect to U-F bond length			
1.976 Å	0.000851		
1.977 Å	0.000019		
1.978 Å	-0.000335		
1.982 Å		0.000499	
1.983 Å		-0.000233	
1.984 Å		-0.000961	
r_e / Å	1.977	1.983	1.996 ^a
HF energy / au	-26260.9964	-28665.8851	
NMR shielding / ppm			
U σ^{dia}	11720.6	12291.9	
U σ^{para}	-50791.1	706.6	
U σ^{tot}	-39070.5	12998.5	

^a Reference 53. ZORA with ECP.

4 Performance

Performance is an essential feature for an integral package. The code of Libcint was intensively optimized for computational efficiency. The optimization includes but is not limited to reusing the intermediates, improving the CPU cache hits, reducing the overhead of function calls, using the sparsity of the transformation matrices. Most of the optimization techniques have already been discussed in Ref 54. Besides, we fixed the memory addresses for most intermediates and stored the addresses in a lookup table. It significantly reduced the CPU addressing time of the high dimension arrays. We didn't adopt the early-contraction scheme as HGP method proposed. Instead, the recurrence relations of DRK's original formula³ was used in the code. Although more FLOPS are needed in our implementation, this choice has advantages on the modern computer architecture. Comparing to the early-contraction scheme, intermediate components I_x , I_y and I_z of DRK's algorithm require less number of variables. As such, more data can be loaded in L1 and L2 cache which reduces the memory access latency. Besides that, I_x , I_y and I_z are more local and aligned in memory. It enabled us to use SSE instructions to parallelize the compute-intensive inner product (7). We found that SSE3 instructions provide 10-30% performance improvements (Table

5). In this regard, SSE3 is always enabled in the following tests.

The performance was measured on ethane molecule at geometry of $R_{C-C} = 1.54 \text{ \AA}$, $R_{C-H} = 1.09 \text{ \AA}$. The tests were carried out on a machine of Intel Core-i5 @ 3.1 GHz 4-core CPU with GCC 4.4.5 and Intel MKL library 10.3 installed. Libcint library was compiled at `-O3 -msse3` level optimization. As a reference, Molpro-2012⁵⁵ (using integral package SEWARD¹⁴) and Psi4⁵⁶ (using integral package Libint⁵⁷) on the same machine were compiled with `gcc -O3` and linked against Intel MKL library with AVX instruction activated.

Table 5: CPU time (in seconds) of computing ERI for ethane molecule.

basis	Basis size	Psi4	Molpro	Libcint	
				w/o SSE3	w/ SSE3
6-31G	30	0.10	0.09	0.09	0.07
6-311G**	72	0.64	0.49	0.49	0.41
ANO	238	2527.6	51.13	53.59	37.78
cc-pVDZ	58	0.45	0.34	0.24	0.21
aug-cc-pVDZ	100	1.87	1.18	1.02	0.85
cc-pVTZ	144	4.98	4.82	2.65	2.05
aug-cc-pVTZ	230	26.03	23.12	12.40	9.27
cc-pVQZ	290	81.24	65.12	31.51	22.60
aug-cc-pVQZ	436	444.23	324.29	151.04	107.24

Table 5 shows the CPU time consumed to compute all basic ERI integrals $(ab|cd)^S$ (8-fold permutation symmetry was assumed) for double, triple and quadruple-zeta basis sets (I/O time is not included). The performance for different basis sets are compared in Figure 1, in which we use MIPS (million integrals per second) to measure the performance. In these tests, Libcint library presents high efficiency for the calculation of the basic ERIs, especially with the loosely contracted basis sets. In the modern multi-processor computer platform, the overall throughput can easily exceed the bandwidth that I/O is able to provide. We tested C_{60} molecule with cc-pVTZ basis (1800 basis functions) on a cluster of 20 CPU cores running @ 2.5GHz. It takes 1321 seconds to generate all (1.3 million million) integrals without using Schwarz inequality, which implies an average bandwidth 7.9 GB/s. In comparison, the bandwidth of disk or network is typically less than 1 GB/s; GPU to CPU data transfer through PCI-express bus is roughly 10 GB/s.

Integrals other than the basic ERI are implemented by the code generator. The performance

of the spherical ERI gradients $(\nabla a b|cd)^S$ on a single CPU core can be found in Figure 1. The performance of integral gradients is better than the basic spherical ERI in the sense that it owns higher MIPS. In 6-311G** and cc-pVDZ bases, the gradients are 67 % (12.5 MIPS vs 7.5 MIPS) and 70 % (10.9 MIPS vs 6.4 MIPS) faster than the basic ERI. In the rest cases, the gradients are 10% - 50 % faster.

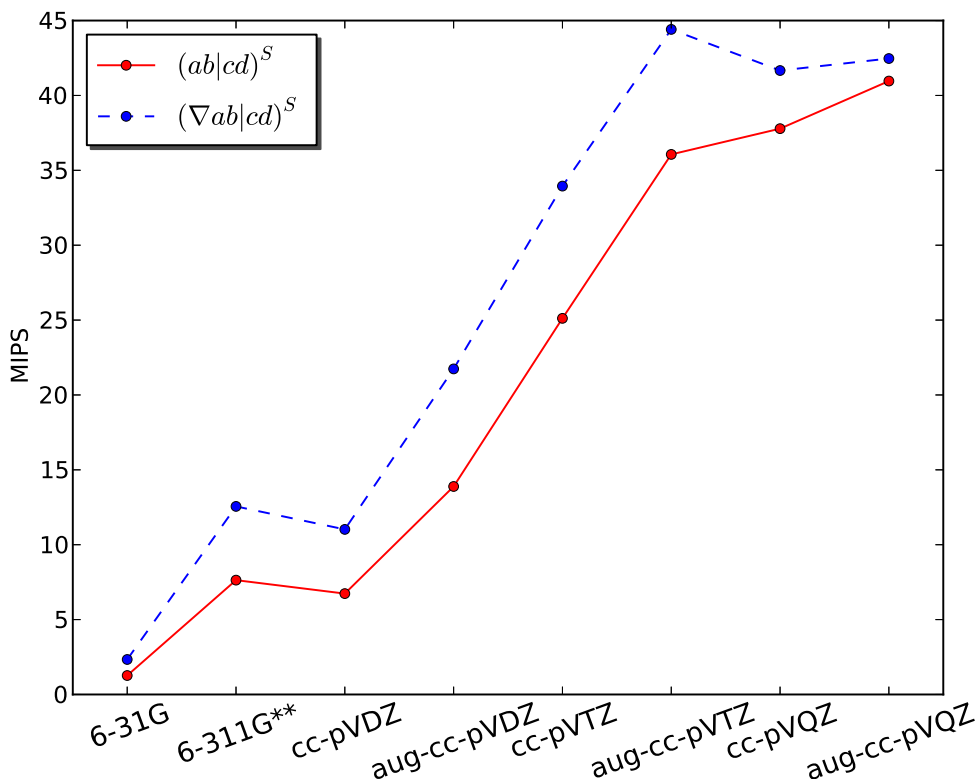


Figure 1: performance of spherical ERI and ERI gradients.

Next, we turn to the performance of spinor integrals. There are two times as many j -adapted spinor functions as spherical functions for a given basis set. For the relativistic theory on top of RKB spinor basis, this results in totally 64 times of the number of spherical integrals to compute (16 times from $(ab|cd)^J$, 16 times from $(\sigma_{\mathbf{p}a} \sigma_{\mathbf{p}b} | \sigma_{\mathbf{p}c} \sigma_{\mathbf{p}d})^J$ and 32 times from $(\sigma_{\mathbf{p}a} \sigma_{\mathbf{p}b} | cd)^J$). Figure 2 shows the real output of the RKB spinor ERIs on a single CPU core. By counting the total number of integrals needed by RKB basis, we can estimate the relative costs of RKB over

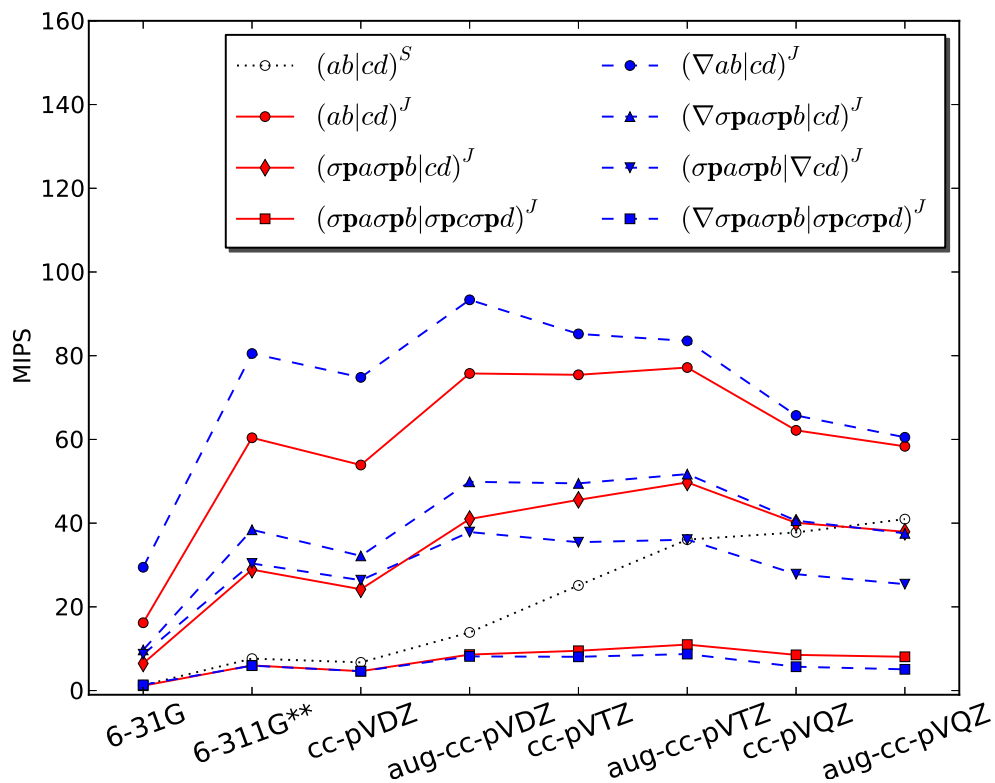


Figure 2: performance of RKB spinor ERI and RKB ERI gradients.

Table 6: Timings of the basic ERI and ERI gradients for spherical functions and RKB spinor functions.

	spherical ERI		RKB spinor ERI	
	basic (s)	gradients ^a	basic ^a	gradients ^b
6-31G	0.07	6.5	25.0	9.5
6-311G**	0.42	7.3	30.8	11.4
cc-pVDZ	0.21	7.3	34.2	11.3
aug-cc-pVDZ	0.87	7.7	39.6	12.1
cc-pVTZ	2.09	8.9	65.2	13.6
aug-cc-pVTZ	9.45	9.8	83.2	14.5
cc-pVQZ	23.19	10.9	110.8	16.5
aug-cc-pVQZ	109.91	11.6	127.0	17.3

^a Data are normalized to the time of basic spherical ERI.

^b Data are normalized to the time of basic RKB spinor ERI.

the regular spherical ERIs, as shown by Table 6. The overall costs of RKB spinor ERI are 25 - 130 times higher than that of spherical ERI. Regarding to the fact that the number of integrals in ERI gradients is 12 times of the number in basic ERIs, the performance of RKB ERI gradients is worse than the spherical case, since the cost ratios for RKB are more than 12 in many tests, while they are all less than 12 for spherical integrals. We also noticed that the more high angular momentum functions a basis set owns, the slower RKB integration tends to be. It reflects the fact that the costs of the RKB ERI are dominated by the inner product (7) since the four \mathbf{p} operators of $(\sigma\mathbf{p}a\ \sigma\mathbf{p}b|\sigma\mathbf{p}c\ \sigma\mathbf{p}d)^J$ introduce $3^4 = 81$ Cartesian intermediates, which implies 81 times of the costs of inner products. This number becomes $3^5 = 243$ for $(\nabla\sigma\mathbf{p}a\ \sigma\mathbf{p}b|\sigma\mathbf{p}c\ \sigma\mathbf{p}d)^J$. As such, the performance decreasing in ERI gradients is more obvious.

5 Summary

The open-source library Libcint provides a new tool to implement integrals for Gaussian type basis functions. With this library, efficiency can be obtained for both human labor and machine costs. By using the built-in symbolic algebra tool, it is simple to implement various types of new integrals, including but not limited to

- arbitrary order of derivatives,
- arbitrary expressions on top of operators \mathbf{p} , \mathbf{r} and σ ,
- nuclear attraction, Coulomb and Gaunt interaction,
- field-dependent basis functions,
- both kinetically and magnetically balanced spinor integrals.

As the numerical examples demonstrated in the present work, the analytical gradients and NMR shielding parameters can be programmed in a simple manner with the integrals generated by the library.

The generality of Libcint library is achieved without losing machine efficiency. On the modern multi-core computers, it is easy to gain an overall throughput being many times of the I/O bandwidth. Based on the present Libcint library, future works can be carried out at least in two aspects. One is to further optimize and port the code for new computer platforms. Another is to improve the symbolic algebra tool for more integral frameworks such as density fitting and multi-particle integrals for explicitly correlated methods.

6 Acknowledgments

The author is grateful to Professor Garnet Chan for his generous support on this project. The author thanks Dr. Lan Cheng for insightful discussions and the comments on the manuscript.

References

- (1) Boys, S. F. *Proc. Roy. Soc. A* **1950**, *200*, 542.
- (2) Dupuis, M.; Rys, J.; King, H. F. *J. Chem. Phys.* **1976**, *65*, 111.
- (3) Rys, J.; Dupuis, M.; King, H. F. *J. Comput. Chem.* **1983**, *4*, 154.
- (4) Pople, J. A.; Hehre, W. J. *J. Comput. Phys.* **1978**, *27*, 161 – 168.
- (5) McMurchie, L. E.; Davidson, E. R. *J. Comput. Phys.* **1978**, *26*, 218 – 231.
- (6) Obara, S.; Saika, A. *J. Chem. Phys.* **1986**, *84*, 3963.
- (7) Obara, S.; Saika, A. *J. Chem. Phys.* **1988**, *89*, 1540–1559.
- (8) Schlegel, H. B. *J. Chem. Phys.* **1982**, *77*, 3676–3681.
- (9) Klopper, W.; Röhse, R. *Theor. Chem. Acc.* **1992**, *83*, 441–453.
- (10) Head-Gordon, M.; Pople, J. A. *J. Chem. Phys.* **1988**, *89*, 5777–5786.

- (11) Gill, P. M. W.; Head-Gordon, M.; Pople, J. A. *Int. J. Quant. Chem* **1989**, *36*, 269–280.
- (12) Gill, P. M. W.; Head-Gordon, M.; Pople, J. A. *J. Phys. Chem.* **1990**, *94*, 5564–5572.
- (13) Gill, P. M. W.; Pople, J. A. *Int. J. Quant. Chem.* **1991**, *40*, 753–772.
- (14) Lindh, R.; Ryu, U.; Liu, B. *J. Chem. Phys.* **1991**, *95*, 5889.
- (15) Lindh, R. *Theor. Chem. Acc.* **1993**, *85*, 423–440.
- (16) Dupuis, M.; Marquez, A. *J. Chem. Phys.* **2001**, *114*, 2067–2078.
- (17) Ishida, K. *J. Chem. Phys.* **1991**, *95*, 5198.
- (18) Ishida, K. *Int. J. Quant. Chem.* **1996**, *59*, 209–218.
- (19) Helgaker, T.; Coriani, S.; Jørgensen, P.; Kristensen, K.; Olsen, J.; Ruud, K. *Chem. Rev.* **2012**, *112*, 543–631.
- (20) Ekström, U.; Visscher, L.; Bast, R.; Thorvaldsen, A. J.; Ruud, K. *J. Chem. Theory Comput.* **2010**, *6*, 1971–1980.
- (21) London, F., *J. Phys. Radium* **1937**, *8*, 397–409.
- (22) Ditchfield, R. *J. Chem. Phys.* **1972**, *56*, 5688.
- (23) Darling, C. L.; Schlegel, H. B. *J. Phys. Chem.* **1994**, *98*, 5855–5861.
- (24) Pyykko, P. *Chem. Rev.* **1988**, *88*, 563.
- (25) Stanton, R. E.; Havriliak, S. *J. Chem. Phys.* **1984**, *81*, 1910.
- (26) Cheng, L.; Stopkowicz, S.; Gauss, J. *Int. J. Quant. Chem.* **2014**, *114*, 1108–1127.
- (27) Cheng, L.; Xiao, Y.; Liu, W. *J. Chem. Phys.* **2009**, *131*, 244113.
- (28) Breit, G. *Phys. Rev.* **1929**, *34*, 553–573.

- (29) Kutzelnigg, W.; Liu, W. *J. Chem. Phys.* **2000**, *112*, 3540–3558.
- (30) Dyllal, K. G.; Jr., K. F. *Chem. Phys. Lett.* **1990**, *174*, 25 – 32.
- (31) Ishikawa, Y.; Jr., R. B.; Sando, K. *Chem. Phys. Lett.* **1983**, *101*, 111 – 114.
- (32) Xiao, Y.; Peng, D.; Liu, W. *J. Chem. Phys.* **2007**, *126*, 081101.
- (33) Yanai, T.; Nakajima, T.; Ishikawa, Y.; Hirao, K. *J. Chem. Phys.* **2002**, *116*, 10122–10128.
- (34) Kelley, M. S.; Shiozaki, T. *J. Chem. Phys.* **2013**, *138*, 204113.
- (35) Sun, Q.; Liu, W.; Kutzelnigg, W. *Theor. Chem. Acc.* **2011**, *129*, 423.
- (36) Titov, A. V.; Ufimtsev, I. S.; Luehr, N.; Martinez, T. J. *J. Chem. Theory Comput.* **2013**, *9*, 213–221.
- (37) Asadchev, A.; Gordon, M. S. *J. Chem. Theory Comput.* **2012**, *8*, 4166–4176.
- (38) Blleloch, G.; Hardwick, J.; Sipelstein, J.; Zagha, M.; Chatterjee, S. *J. Parallel Distributed Comput.* **1994**, *21*, 4 – 14.
- (39) Yasuda, K. *J. Comput. Chem.* **2007**, *29*, 334.
- (40) Asadchev, A.; Allada, V.; Felder, J.; Bode, B. M.; Gordon, M. S.; Windus, T. L. *J. Chem. Theory Comput.* **2010**, *6*, 696–704.
- (41) Luehr, N.; Ufimtsev, N.; Martínez, I. S.; J, T. *J. Chem. Theory Comput.* **2011**, *7*, 949.
- (42) Sun, Q. Libcint library. <https://github.com/sunqm/libcint.git>,
A simple SCF program engined by Libcint library can be found in
<https://github.com/sunqm/pyscf.git>.
- (43) Dyllal, K. G. *Theor. Chem. Acc.* **2002**, *108*, 335.
- (44) Shiozaki, T. *J. Chem. Theory Comput.* **2013**, *9*, 4300–4303.

- (45) Wang, F.; Li, L. *Journal of Computational Chemistry* **2002**, *23*, 920–927.
- (46) Komorovskó, S.; Repiskó, M.; Malkina, O. L.; Malkin, V. G.; Ondk, I. M.; Kaupp, M. *J. Chem. Phys.* **2008**, *128*, 104101.
- (47) Xiao, Y.; Sun, Q.; Liu, W. *Theor. Chem. Acc.* **2012**, *131*, 1080, 10.1007/s00214-011-1080-z.
- (48) Ehlers, A. W.; Ruiz-Morales, Y.; Baerends, E. J.; Ziegler, T. *Inorg. Chem.* **1997**, *36*, 5031–5036.
- (49) Schreckenbach, G.; Ziegler, T. *Int. J. Quant. Chem.* **1997**, *61*, 899–918.
- (50) Jost, A.; Rees, B. *Acta. Crystallogr. B* **31**, 2649.
- (51) Barnes, L. A.; Liu, B.; Lindh, R. *J. Chem. Phys.* **1993**, *98*, 3978–3989.
- (52) Bouten, R.; Baerends, E. J.; van Lenthe, E.; Visscher, L.; Schreckenbach, G.; Ziegler, T. *J. Phys. Chem. A* **2000**, *104*, 5600–5611.
- (53) Schreckenbach, G. *International Journal of Quantum Chemistry* **2005**, *101*, 372–380.
- (54) Flocke, N.; Lotrich, V. *J. Comput. Chem.* **2008**, *29*, 2722–2736.
- (55) Werner, H.-J. et al. MOLPRO, version 2012.1, a package of ab initio programs. 2012; see <http://www.molpro.net>.
- (56) Turney, J. M. et al. *WIREs: Comput. Mol. Sci.* **2012**, *2*, 556–565.
- (57) Valeev, E. F. Libcint library. <http://www.chem.vt.edu/chem-dept/valeev/libint/>.

